JOC The Journal of Organic Chemistry
Article
pubs.acs.org/joc

Structural Dynamics of Overcrowded Alkene-Based Molecular Motors during Thermal Isomerization

Arjen Cnossen, Jos C. M. Kistemaker, Tatsuo Kojima, and Ben L. Feringa*

Stratingh Institute for Chemistry and Zernike Institute for Advanced Materials, Faculty of Mathematics and Natural Sciences, University of Groningen, Nijenborgh 4, 9747AG Groningen, The Netherlands

Ⓢ *Supporting Information*

ABSTRACT: Synthetic light-driven rotary molecular motors show complicated structural dynamics during the rotation process. A combination of DFT calculations and various spectroscopic techniques is employed to study the effect of the bridging group in the lower half of the molecule on the conformational dynamics. It was found that the extent to which the bridging group can accommodate the increased folding in the transition state is the main factor in rationalizing the differences in barrier height and, as a consequence, the rotary speed. These findings will be essential in designing future rotary molecular motors.

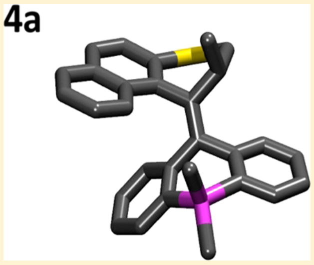

■ INTRODUCTION

Molecular machines including rotary motors have the potential to play a central role in nanotechnology.[1−4] In recent years, many different kinds of rotary molecular motors have been reported, powered by light,[5] chemical energy,[6,7] electricity,[8−10] or a combination of these.[11,12] The molecular motors developed in our group are based on sterically overcrowded alkenes.[5] Understanding the mechanism of their rotation is crucial for optimization of their function and application. Our 'second generation' molecular motors typically consist of a tricyclic lower half or 'stator' connected via a double bond to a chiral, naphthalene-substituted (hetero)cyclic upper half that acts as a 'rotor' (e.g., **1**−**4**, Chart 1).[13,14] These compounds undergo repetitive unidirectional rotation of the upper half relative to the lower half under the influence of UV irradiation and heat. The UV light powers an *E*−*Z* isomerization, which leaves the compound in a thermodynamically unfavorable conformation.[13] A thermally activated helix inversion relieves steric hindrance and brings the molecule back to its initial, most stable conformation (Scheme 1).

Chart 1. Molecular Motors 1−4 and Bistricyclic Enes 5 and 6

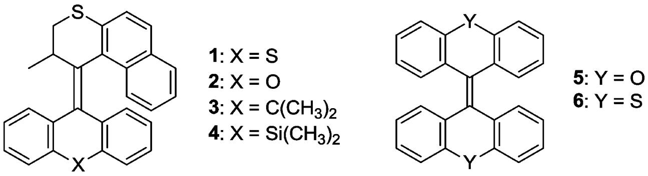

Sterically overcrowded alkenes (e.g., **5** and **6**, Chart 1) can interconvert between a broad spectrum of conformations, as has been studied thoroughly by Agranat and co-workers.[15] A combination of experimental and computational chemistry has been used to study this type of compounds and their properties.[16−20] Second generation molecular motors show similar conformations, where folding of the upper and lower half and twisting around the double bond relieve steric strain in the molecule. During the rotation process, there are many intermediates with different degrees of folding and twisting, resulting in a complex, dynamic conformational behavior.

Structural modifications can have a large impact on the rotary processes of these types of molecular motor, as was observed upon replacing the methyl group at the stereogenic center or when the naphthalene part of the upper half was truncated.[21] Similarly, the conformational dynamics of bistricyclic (aromatic) enes are sensitive to the nature of the bridging group.[15] However, it was observed experimentally that the bridging atom X in the lower half of motors **1**−**3** has a relatively small effect on the rate of thermal helix inversion.[13] The reason for this is not entirely clear. Different bridging groups have different bond lengths and angles; therefore a change in conformational stability is expected. Evidently, this does not strongly affect the rate-determining step of the thermal helix inversion. This shows that while we have learned a great deal about how these motors operate,[21,22] not all factors influencing the rotation are fully understood, and further in-depth investigations are warranted.

Here we present an experimental study of both the thermal isomerization and the photochemistry of a series of second generation molecular motors in combination with density functional theory (DFT) calculations. Molecular motor **1** has been studied extensively, and its rotary processes have been examined in detail both in solution[13,14,23] and on gold nanoparticles.[24] Furthermore, it has been used in more complex systems, albeit with varying degrees of success.[25,26] The results obtained for **1** can be used as a benchmark to validate the results of the DFT calculations, and the methodology can be

Received: October 15, 2013
Published: January 12, 2014

dx.doi.org/10.1021/jo402301j | *J. Org. Chem.* 2014, 79, 927−935

Scheme 1. Isomerization Processes of 1−4 upon UV Irradiation at 312 nm and Subsequent Heating

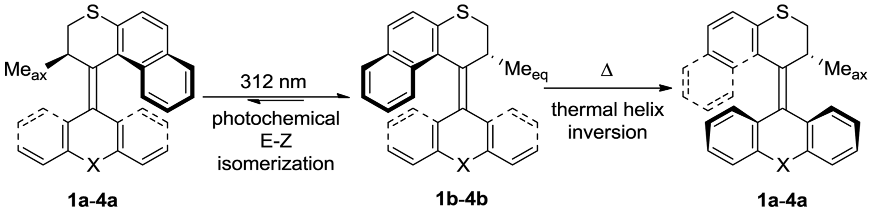

Scheme 2. Synthesis of Molecular Motor 4

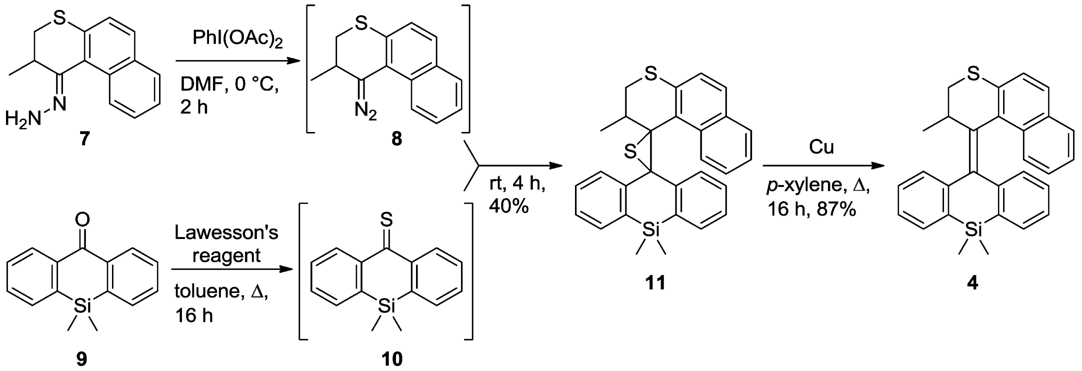

extended to the other compounds in the series. Compounds **2** and **3** were reported to act as molecular motors previously but have not been studied extensively.[13] The introduction of a silicon bridging group in compound **4** further extends this series of motors. The replacement of sulfur by a dimethyl silyl bridging group in thioxanthene derivatives is known to yield geometrically similar structures, but increased folding is observed.[27] This could have an effect on the rate of thermal helix inversion as during the thermal helix inversion the naphthalene part slips over the lower half. The more the lower half is folded, the more facile this slipping process takes place, thereby allowing for faster rotation. Also, a ring flip occurs in the lower half, which may be affected by the variations in the bridging group. The effect of the bridging group on photochemical isomerization has to date received little attention in this regard. This study is expected to provide greater insight into the structures of the intermediates involved in the rotary action of the molecular motor and how the structural and dynamic properties are affected by the nature of the bridging group. A better understanding of the rotation and the structural parameters will help in the design of molecular motors and their incorporation into more sophisticated multicomponent systems.

■ RESULTS AND DISCUSSION

Synthesis. The synthesis of compounds **1**−**3** was reported previously.[13] The synthesis of compound **4** is summarized in Scheme 2. The key step in the synthesis of second generation molecular motors is the introduction of the sterically overcrowded olefinic bond, which is generally achieved using a Barton−Kellog coupling reaction. Precursors **7** and **9** are known compounds and were synthesized according to literature procedures in three[13] and seven[27,28] steps, respectively. Hydrazone **7** was oxidized to the corresponding diazo compound **8** with phenyliodine diacetate at 0 °C. In parallel, the ketone functionality in **9** was converted to the thioketone using Lawesson's reagent. Both **8** and **10** are highly reactive compounds that should not be stored but were found to react together at room temperature to form episulfide **11** in 40% yield. Desulfurization occurs upon treatment with copper bronze in refluxing *p*-xylene to yield molecular motor **4**. Compound **4** was characterized by ^{1}H and ^{13}C NMR as well as HRMS. In the ^{1}H NMR spectrum, the typical coupling patterns for the hydrogen atoms of the substituted thiopyran ring were observed. The two methyl groups on silicon are not equivalent, as one adopts a (pseudo)axial conformation toward the naphthalene unit, whereas the other is in an equatorial position, pointing away from the rest of the molecule. This results in Me signals in the ^{13}C NMR spectrum at −4.4 and −1.1 ppm.

Conformational Analysis. Geometry optimizations of motors **1**−**4** were performed on the B3LYP/6-31G(d,p) level of theory, which has previously been used to provide reliable results for geometries and energies of overcrowded alkenes.[29,30,34,35] Compound **1** is known to exist in an *anti*-folded conformation as its global energy minimum (Chart 2a), from earlier DFT calculations[34,35] and X-ray analysis.[13] In this *anti*-folded structure steric hindrance is relieved by folding away the upper and lower half in opposite directions with respect to the central double bond. Similar folded structures were found for **2**−**4**: the tricyclic lower half is folded to the back, and the naphthalene part points forward, with the methyl group in an axial orientation to minimize steric interactions. Some key structural parameters are collected in Table 1.

The conformation of the upper half of these molecules is nearly identical in all cases and does not seem to be influenced significantly by the lower half. The central carbon−carbon double bond has a bond length of 136 pm, which is only slightly elongated compared to 134 pm for a normal carbon−carbon double bond. Although the compound appears strained, there is little pyramidalization (Chart 2c) at the carbon atoms of the double bond; the strain is mostly relieved by folding of upper and lower parts. In the upper half this is reflected by the axial position of the methyl group. In the lower half the angle between the two phenyl rings deviates significantly from 180° (folding angle 129−144°). Differences are introduced here because of different bond lengths to the bridging groups and

Chart 2[a]

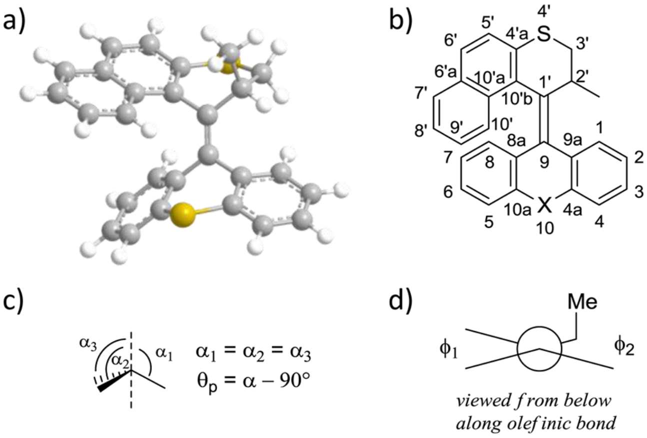

[a](a) Geometry optimized structure of **1**. (b) Numbering scheme adopted for **1**−**4**. (c) Definition of pyramidalization angle θ_p. (d) Schematic representation of dihedral angles ϕ_1 and ϕ_2 over the C9−C1′ bond.

Table 1. Calculated Bond Lengths and Angles for Motors 1−4

motor	θ_p C1′ (deg)	θ_p C9 (deg)	ϕ_1 (deg)[a]	ϕ_2 (deg)[b]	C1′−C9 (Å)	folding (deg)[c]
1	0.678	0.684	1.21	6.32	1.36	132
2	1.02	1.54	0.252	9.97	1.36	144
3	0.878	0.209	6.70	2.57	1.36	132
4	0.800	0.0762	4.23	1.48	1.36	129

[a]C10′b−C1′−C9−C8a. [b]C2′−C1′−C9−C9a. [c]Angle between the two phenyl rings in the lower half.

differences in preferred bond angles. Incidentally, compound **2** which shows the least folding, also shows the largest pyramidalization at C9. It is noteworthy that for the dihedral angles C10′b−C1′−C9−C8a and C2′−C1′−C9−C9a at the double bond (ϕ_1 and ϕ_2, Chart 2d) in **1** and **2** a very low torsion angle is observed at the naphthalene side. For compounds **3** and **4**, the pseudoaxial methyl substituent on the bridging group experiences steric hindrance from the naphthalene moiety, and the dihedral angle at that side is the largest.

Photoisomerization. Irradiation of compounds **1a**−**4a** in *n*-hexane at 312 nm results in a photochemical *E*−*Z* isomerization. As a consequence nearly one-half rotation of the upper half relative to the lower half takes place, and the thermally unstable isomers **1b**−**4b** are generated, with the methyl group in an unfavorable equatorial position (Scheme 1). This process can be followed by UV−vis absorption, CD, and ^{1}H NMR spectroscopy.

In the UV−vis absorption spectra of **1**−**4** in *n*-hexane a decrease in the absorption around 350 nm is observed upon irradiation at 312 nm (Figure 1). For **1**, **3**, and **4** this is accompanied by an increase in absorption in the 250−275 nm range, and for **2** an increase around 300 nm is observed. Clear isosbestic points are observed, which indicates a unimolecular process takes place. At room temperature, thermal relaxation is not observed within 1 h. Heating the solution to 70 °C overnight results in the full reversal of the spectral changes.

The quantum yield for the photoisomerization of **1**−**4** was determined by irradiation (312 ± 1 nm) of a concentrated solution in toluene. The conversion to unstable **1b**−**4b** was followed by UV−vis absorption spectroscopy at 375 nm ($0.1 < A < 1$). The rate of conversion was then compared to the rate of decomposition of ferrioxalate under the same conditions of irradiation according to standard procedures[31] to give the quantum yield for photoisomerization (Table 2).

The quantum yields for photoisomerization are all low, between 0.55% and 1.6%, presumably because there is a favorable pathway for internal conversion available from the excited state. Furthermore, **1**−**4** all show fluorescence, which competes with photoisomerization. For motor **2** the quantum yield for the reverse reaction is even higher than for the forward reaction. In the end, this would mean that the efficiency for the rotation is low, but as long as the thermal helix inversion takes place, the rotation remains unidirectional.[23,32]

Enantiomerically pure material for CD spectroscopy was obtained by chiral stationary phase HPLC (see Experimental Section). Due to the steric overcrowding around the central double bond, molecules **1a**−**4a** cannot be flat but adopt a helical shape. This is expressed in the CD spectrum by a strong band between 250 and 300 nm and a weaker band of opposite sign at ca. 350 nm (Figure 2). Upon irradiation, a photoequilibrium is established between the initial thermodynamically stable form and the respective unstable form **1b**−**4b**, which have opposite helicity. For **1**, **3**, and **4** this is seen as an inversion of the major bands in the CD spectrum. For **2**, a complete inversion is not observed because the photostationary state (PSS) is relatively rich in **2a**; instead a reduction in intensity of the signal due to the formation of **2b** is observed. Assignment of the absolute stereochemistry from the CD spectra of the stable and unstable form was achieved using time-dependent (TD) DFT with the B3LYP functional and the 6-31G++(d,p) basis set. The calculated spectra are overlaid with the experimental spectra (Figure 2). Since it is known that this method has a systematic deviation in the excitation energies,[33] the calculated spectra were shifted by 15 nm to better show the agreement with the experimental data. Furthermore, the spectra were normalized to the strongest absorption band in the spectrum of compound **4**.

The overall shapes of the calculated CD spectra fit reasonably to the experimental data. Two main factors should be considered to explain the deviations. In the first place, the calculations simulate the compound in the gas phase, whereas the measurements are conducted in solution. Second, it is likely that there are multiple conformations that contribute to the experimental CD spectrum. The predicted spectrum is the spectrum of the molecule in its lowest energy conformation, but it cannot be excluded that there are several conformations that are close in energy and thus are present under experimental conditions that have a significantly different contribution to the overall CD spectrum. The results of the calculations are, however, sufficient to discriminate between the two possible helicities and can be used to assign the absolute stereochemistry.

Thermal Relaxation. After photoisomerization, the motor is present in a thermodynamically unfavorable conformation. A thermal helix inversion relieves steric strain and allows the molecule to reach its structure of minimum energy again (**1a**−**4a**). Computational studies of this process have been reported for compound **1**.[34,35] Our calculations confirm these results to a large extent, revealing the same intermediates and transition states; however, we find that their order is different as well as their relative energies.

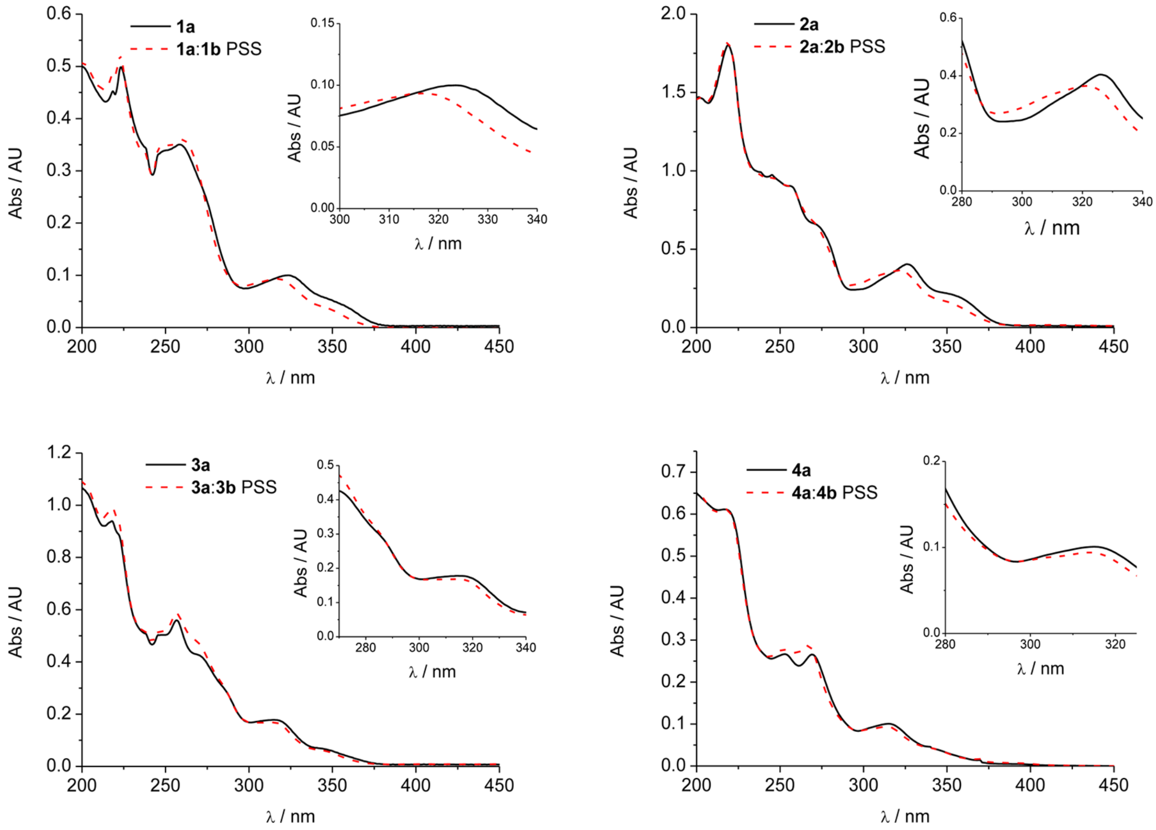

Figure 1. UV−vis absorption spectra in *n*-hexane of **1a**−**4a** (black lines) and the PSS mixture of **1a**−**4a** and **1b**−**4b** obtained after irradiation at 312 nm (red dashed lines).

Table 2. Parameters for the Photochemical Conversion of 1a−4a to 1b−4b (Toluene Solution, λ = 312 nm)

motor	PSS ratio[a]	$\Phi_{a\to b}$[b] (%)	$\Phi_{b\to a}$[c] (%)
1	8:92[d]	1.6	0.91
2	38:62	0.55	0.75
3	8:92[d]	1.5	0.17
4	19:81	0.83	0.12

[a] Determined by ^{1}H NMR spectroscopy in toluene-d_8. [b] Determined by ferrioxalate actinometry. [c] Calculated from PSS ratio and $\Phi_{a\to b}$. [d] From ref 13.

Two possible pathways were established for the thermal helix inversion, A and B. In both pathways the same steps occur, but in a different order (Figure 3). In both pathways, an initial ring flip in the thiopyran of the upper half (TS1) brings the methyl group on the stereogenic center from an equatorial to an axial position, reaching the *anti*-folded, twisted intermediate I1. This intermediate is common to both pathways. For pathway A, the upper half subsequently slips over the lower half via TS2 to give twisted *syn*-folded I2, and finally a ring flip in the lower half leads via TS3 to the global energy minimum, *anti*-folded **1a**. In pathway B, the order of these two steps is inverted: first a ring flip in the lower half occurs to reach *syn*-folded twisted I3, and then the upper half slips past the lower half. In both cases the rate-determining step was found to be the one in which the naphthalene moiety of the upper half slips over the lower half, going through transition state TS2 or TS6 in pathway A and B, respectively.

Another intermediate I4 (Figure 4a) was found, which was reported previously to be an intermediate in the thermal helix inversion of **1**.[35] This intermediate can indeed be reached from I3: a ring flip in the upper half brings the methyl group from an axial position back to an equatorial position. However, when calculating the intrinsic reaction coordinate (IRC) for the rate-determining transition state TS6, it turned out that I4 is not on the minimum energy pathway for motor **1**. Rather, I4 represents a conformational cul-de-sac and to reach the global energy minimum **1a**, it needs to go back through I3 (Figure 4b).

Intermediates and transition states of similar geometry were found for motors **2** and **3**, although there are differences in relative energies. Whereas the pathways for thermal helix inversion for motors **1**−**3** are similar, motor **4** deviates somewhat. In pathway A, the same intermediates were found, but TS2 does not connect I2 and I1. When the intrinsic reaction coordinate was calculated for TS2, it was found that TS2 does not connect to I1 but rather goes directly to **4b**. A minimum with the geometry of I1 does still exist but is not on the minimum energy pathway. From I2 a ring flip in the lower half takes place, and **4a** is reached via TS3, as for motors **1**−**3**. In pathway B, an intermediate with a geometry similar to I3, in which the methyl group at the stereogenic center is in an axial orientation, could not be found. In this pathway, I1 is directly connected to I4 (Figure 4b). Intermediate I4 is not a conformational cul-de-sac for motor **4** as it is for **1**−**3** but rather leads to the global energy minimum **4a** via TS6 (Figure 6).

Since different intermediates for motor **4** were found than for **1**−**3**, calculation of the complete reaction pathway for the thermal helix inversion was carried out (Figure 5). In the IRC of pathway A a leveling off can be seen close to the geometry of I1, as indicated by the arrow, but this intermediate is not on the

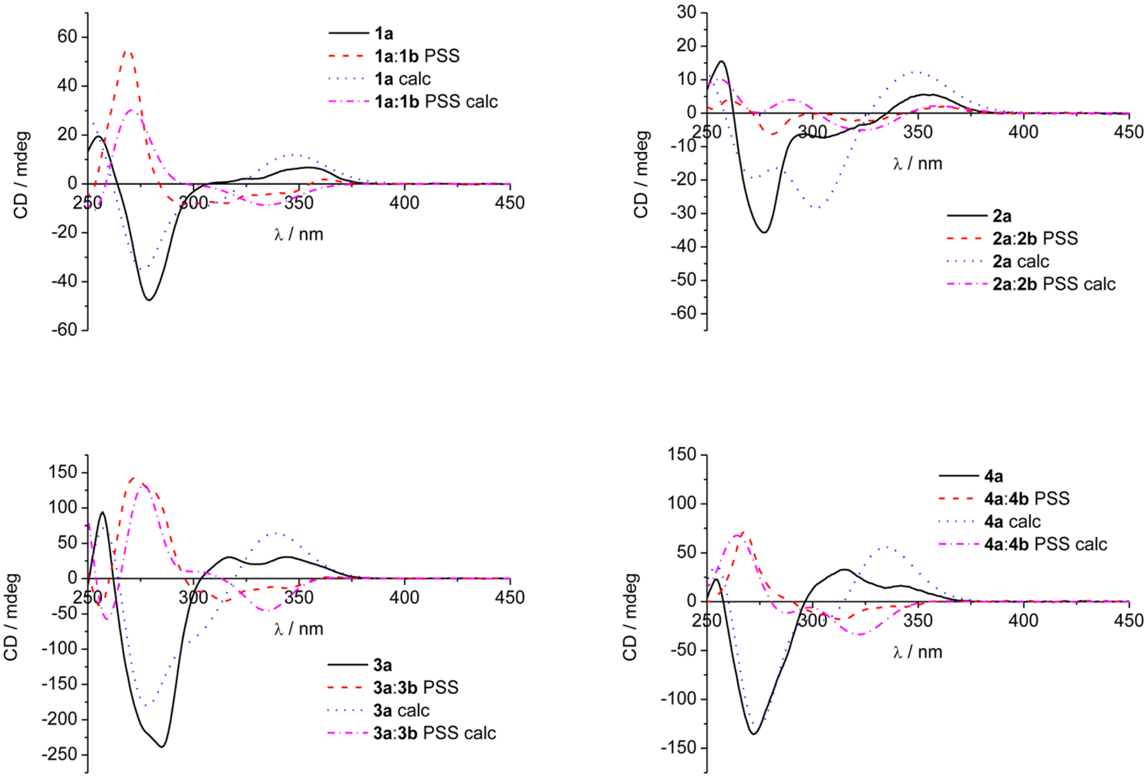

Figure 2. CD spectra in *n*-hexane of **1a**–**4a** (black lines) and the PSS mixture of **1a**–**4a** and **1b**–**4b** obtained after irradiation at 312 nm (red dashed lines) compared to the calculated CD spectra of **1a**–**4a** (blue dotted lines) and the PSS mixture (magenta dot-dash lines).

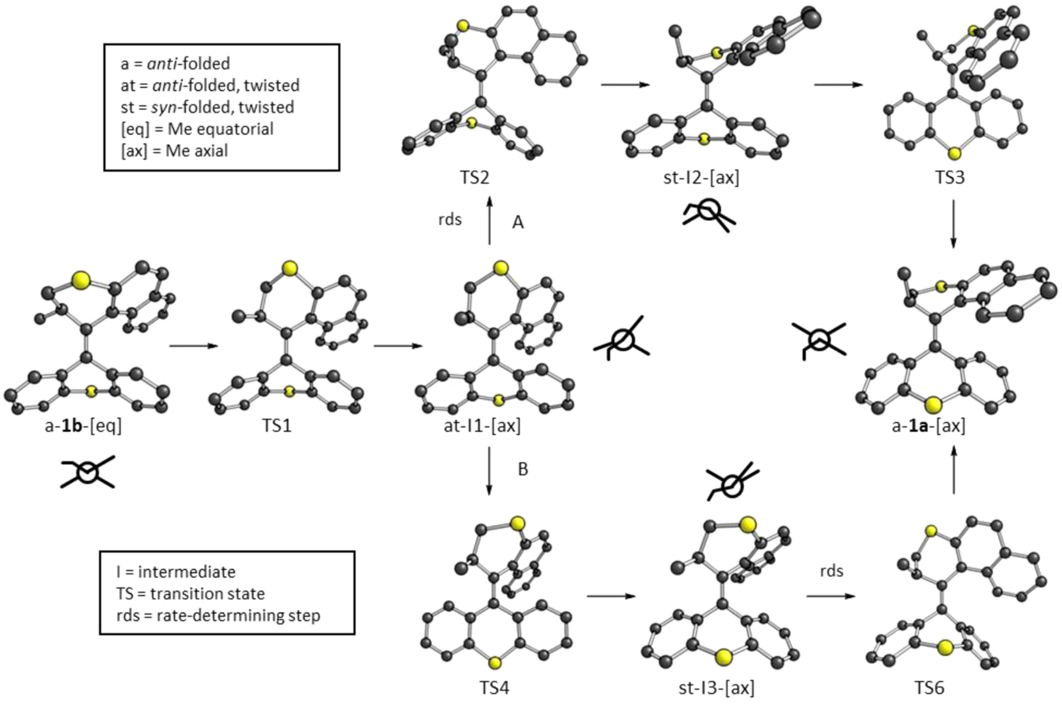

Figure 3. Thermal conversion from unstable **1b** to stable **1a** via pathways A (top) and B (bottom). With all intermediates a schematic top view of the molecule along the olefinic double bond is drawn. The rate-determining ring flip in the upper half is indicated with rds.

minimum energy pathway. Similarly, in pathway B the curve levels off close to I3, indicated by the arrows, but this is not the a true minimum. With a ring flip in the upper half the methyl group is brought to an equatorial conformation, reaching a minimum in I4. From intermediate I4, a similar geometry is again adopted on the path to TS6. The IRC of both pathway A and pathway B are available as a movies.

The energy of all the transition states and intermediates was calculated and plotted to compare motors **1**–**4** with each other (Figure 6). The stable forms **1a**–**4a** were normalized at 0 kJ/

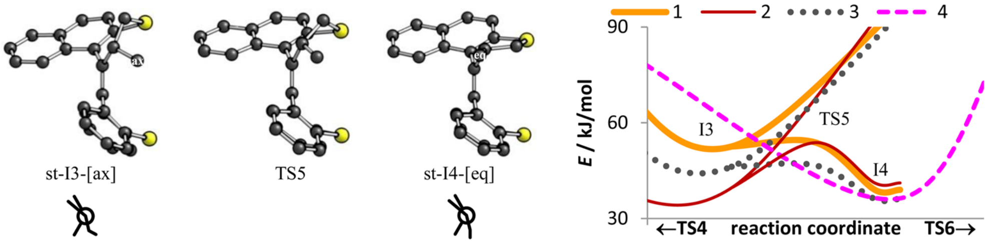

Figure 4. (Left) Conversion of *syn*-folded I3 with the methyl group in an axial orientation through TS5 to *syn*-folded I4 with the methyl group in an equatorial orientation. (Right) Energy profile along the reaction coordinate for the conversion of I3 to I4 via TS5.

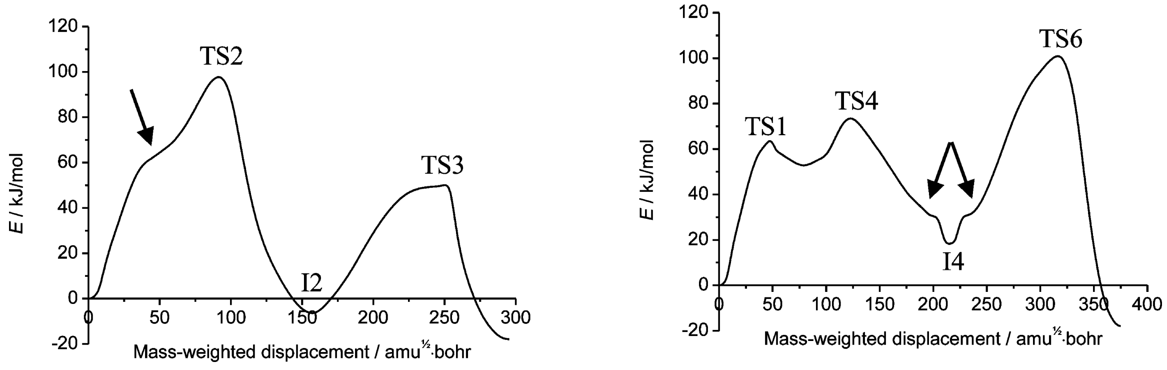

Figure 5. Minimum energy pathway A (upper) and B (lower) for the thermal helix inversion of **4b** to **4a** calculated with stride 0.5 amu$^{1/2}$ Bohr.

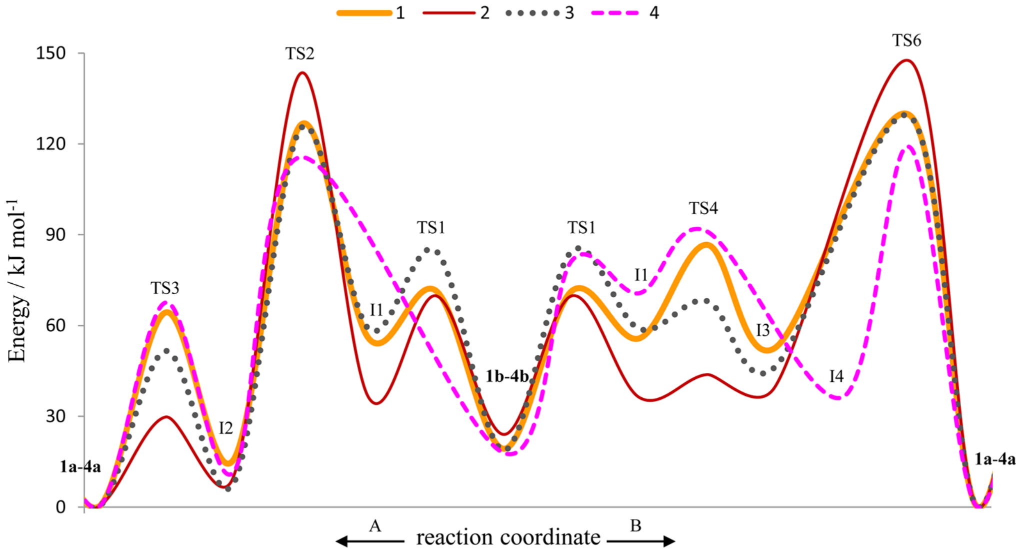

Figure 6. Energy profile along the reaction coordinate for thermal helix inversion of motors **1**−**4**.

mol, which allows for ready comparison of the energy barriers. In all cases, pathway A was found to have a slightly lower energy than pathway B, contrary to what was reported previously for motor **1**.[35] However, the difference is only ca. 4 kJ/mol. Compared to compound **1** the transition states in which either the upper or the lower half undergoes a ring flip are significantly lower in energy for compound **2**.

However, the rate-determining transition states TS2 and TS6, in which the naphthalene upper half moves over the lower half, are higher in energy. This can be rationalized by the small folding angle of the oxygen-bridged lower half: it inverts readily but does not fold away enough to let the upper half slip past. For compound **3** the rate-determining transition states have the same energy as for **1**. The transition state TS1 for the initial ring flip in the upper half of **3** was found to be higher in energy, despite the fact that hardly any structural change takes place in the lower half during this step. The ring flip in the lower half on the other hand has a lower barrier. In the series **1**−**4**, silicon-bridged motor **4** has the lowest barrier for the rate-determining step. Due to the increased folding in the lower half the naphthalene upper half can easily slip past.

The energy barriers calculated with DFT can be compared to the experimentally obtained Gibbs free energy of activation ($\Delta^{\ddagger}G°$) for the thermal relaxation of **1b**−**4b**. For motors **1**−**3**, $\Delta^{\ddagger}G°$ for the thermal isomerization was reported previously; for compound **4** it was determined to be 93.3 kJ/mol (see Supporting Information).

The calculated barriers are in good agreement with experimentally determined data, with the exception of **2**, for which the calculated value is 19 kJ/mol higher than the

Table 3. Barriers for Thermal Helix Inversion of 1b–4b to 1a–4a

motor	(measured)$\Delta^{\ddagger}G°$ (kJ/mol)	SCF energy (kJ/mol) (calcd B3LYP)	$\Delta^{\ddagger}G°$ (kJ/mol) (calcd B3LYP)	$\Delta^{\ddagger}G°$ (kJ/mol) (calcd M06-2X)
1	106[a]	107	110	119
2	100[a]	119	123	130
3	106[a]	106	110	117
4	93.3	97.8	99.8	108

[a] From ref 13.

measured barrier (Table 3). The calculated barrier could be invalid, but this is unlikely as the calculations show a good correspondence with the measured data for the other compounds. The consideration of dispersion forces is regarded as a significant deficiency in general DFT methods, which are improved upon by the implementation of (long-range) dispersion corrections.[36] In an attempt to improve on the slight overestimation of the thermochemical results obtained with B3LYP/6-31G(d,p), all transition states of significance (TS2 and TS6) and the unstable states (**1b**–**4b**) were investigated also using M06-2X/6-31G(d,p), which resulted in a larger deviation of activation energy when compared to the experimental results (see Table 3; for additional calculations on motor **1** using different dispersion corrections, see Supporting Information). A more probable explanation for the observed error of **2** is that there is an additional process with a lower barrier, such as thermal *E*–*Z* isomerization. The barrier for thermal *E*–*Z* isomerization of dixanthylene **5** is around 75 kJ/mol,[37] which is considerably lower than for dithioxanthylene **6** (115 kJ/mol[16]). In that case, the main factor for a low barrier to thermal *E*–*Z* isomerization was proposed to be ground state destabilization.[15] If in the present case the barrier for thermal *E*–*Z* isomerization is also relatively low, this would explain the results obtained. That would also imply that **2** does not in fact act as a molecular motor but rather switches back and forth between two states. To confirm this, the barrier for thermal *E*–*Z* isomerization should be calculated. Furthermore, from an experimental point of view, the molecule should be unsymmetrically substituted in the lower half in a way that allows discrimination of the thermal helix inversion and the thermal *E*–*Z* isomerization pathways. A detailed study of thermal *E*–*Z* isomerization in compound **2** is currently underway.

The barrier for thermal helix inversion of the unstable form of **4** is lower than for the other motors in the series. Compound **4** shows the largest folding in the lower half, which facilitates the slipping of the upper half over the lower half in the rate-determining step in the thermal helix inversion. This trend seems to hold for the other motors in the series; however, this pertains to the geometry in the ground state. Considering the folding of the lower half for the different motors in the unstable form going to the transition state, the folding increases by 20° in all cases (Table 4). A more appropriate explanation for the differences in thermal isomerization is that the differences in the barriers are dependent on how well the bridging group can accommodate the extra folding that is needed to reach the transition state.

Table 4. Folding of the Lower Half in 1b–4b and TS2

motor	folding in TS2 (deg)	folding in **1b**–**4b** (deg)
1	110	128
2	118	139
3	110	128
4	106	125

■ CONCLUSIONS

The photochemical and thermal isomerization processes of a series of second generation molecular motors were characterized and studied with UV–vis absorption, CD, and NMR spectroscopy. Various bridging groups in the lower half influence the process of rotation because of small differences in conformation. Motors **1**–**4** undergo photochemical *E*–*Z* isomerization upon UV irradiation (312 nm). This process can be followed using UV–vis absorption and CD spectroscopy, which shows the formation of the corresponding unstable forms with opposite helicity. This was supported by TD-DFT calculations, which also allow us to assign the absolute stereochemistry of the enantiomers. The photochemical quantum yields of photoisomerization were determined to be in the range of 0.5–1.6%. For compound **2** the quantum yield for the 'reverse' reaction was found to be higher than the 'forward' direction. Still, a favorable PSS can be obtained because of the difference in absorption between the stable and the unstable form at the wavelength of irradiation.

The thermal relaxation of the unstable form of motors **1**–**4** was modeled using DFT calculations. Two pathways for thermal helix inversion were established for these motors. In both pathways compound **2** has the highest barrier and the silicon-bridged motor **4** the lowest. This latter motor behaves somewhat differently compared to the other compounds, in that its thermal helix inversion proceeds via different intermediates. However, the transition state of the rate determining step still has similar geometry to that of motors **1**–**3**.

There is a good agreement between the calculated energy barrier and the Gibbs free energy of activation for the thermal relaxation for motors **1**, **3**, and **4**. For compound **2**, the barrier calculated for the thermal helix inversion is significantly higher than the empirical value of $\Delta^{\ddagger}G°$ for thermal relaxation that was measured. Most probable, thermal relaxation of the unstable form of **2** does not proceed via helix inversion. A possible alternative is thermal *E*–*Z* isomerization, which would compromise the rotation process. However, further investigation is necessary to confirm this.

A clear correlation between the ground state geometries and the $\Delta^{\ddagger}G°$ for thermal helix inversion could not be found. The folding angle in the lower half gives an indication, however, that the main factor is the energy cost to increase the degree of folding to the level needed in the transition state. This energy cost is lowest for the silicon-bridged motor **4**, which also shows the most folding in the lower half in the ground state.

Overall, our understanding of the rotation process of these second generation molecular motors has greatly increased by combining experimental work with computational data. The DFT calculations allow for visualization of the conformational behavior and can predict geometries of intermediates and transition states and their energy. This work will help in designing and identifying new motor topologies to explore and to understand how to incorporate them into more advanced systems to take advantage of their unique dynamics.

■ EXPERIMENTAL SECTION

General Procedures. Unless stated otherwise all reagents were obtained from commercial sources and used as received without further purification. Solvents for reactions were reagent grade and distilled and dried according to standard procedures. Reactions were performed under a nitrogen atmosphere. Column chromatography was performed on silica gel (230−400 mesh) using positive pressure. Chemical shifts are denoted in δ-units (ppm) relative to the residual solvent peak ($CDCl_3$: ^1H $\delta = 7.26$, ^{13}C $\delta = 77.0$; DMSO: ^1H $\delta = 2.49$, ^{13}C $\delta = 39.5$). HRMS (ESI+) spectra were obtained with a LTQ Orbitrap XL.

5,5-Dimethyl-5,10-dihydrodibenzo[b,e]siline. This compound was prepared via a modified literature procedure:[28] to a solution of bis(2-bromophenyl)methane (12 g, 37 mmol) in Et_2O (150 mL) was added a solution of *n*-BuLi (1.6 M in hexane, 50 mL, 77 mmol) at 0 °C. The resulting yellow mixture was stirred for 1 h at 0 °C followed by the dropwise addition of dichlorodimethylsilane (5.3 mL, 44 mmol) at −78 °C. The cooling bath was removed, and the mixture was stirred overnight. The resulting colorless precipitate was removed by filtration and washed with Et_2O. The organic layer was washed with water and dried on Na_2SO_4. The removal of the organic solvent gave 9.4 g of the title compound with high enough purity for the next reaction. ^1H NMR (300 MHz, $CDCl_3$) δ 0.54 (s, 6H), 3.98 (s, 2H), 7.12−7.31 (m, 4H), 7.35 (d, $J = 7.0$ Hz, 2H), 7.56 (dd, $J = 6.7$, 1.6 Hz, 2H).

Episulfide ***11***. A mixture of ketone **9** (0.30 g, 1.3 mmol) and Lawesson's reagent (0.61 g, 1.5 mmol) in toluene (8 mL) was heated at reflux for 15 h. After filtration of the precipitate the solvent was removed under reduced pressure. The residue was dissolved in a minimum amount of dichloromethane and absorbed immediately onto silica (1 g) under reduced pressure. This was loaded onto a small silica column (3 g), and a blue band was rapidly eluted with pentane to yield 0.15 g of impure thioketone **10** as a blue solid. Compound **8** is unstable under ambient conditions and was used immediately without any further purification. In parallel, to a solution of hydrazone **7** (0.15 g, 0.63 mmol) in DMF (10 mL) at 0 °C was added $PhI(OAc)_2$ (0.20 g 0.63 mmol). The resulting mixture was stirred for 2 h at 0 °C and then transferred into the flask containing thioketone **10**. The resulting solution was stirred for 7 h at rt and poured into water, followed by extraction with ethyl acetate. The organic layer was washed with water three times and dried on Na_2SO_4. The solvents were removed under reduced pressure followed by column chromatography (SiO_2, pentane) yielding episulfide **11** (0.12 g, 40% based on hydrazone **7**) as a colorless solid. ^1H NMR (400 MHz, $CDCl_3$) δ 0.18 (s, 3H), 0.87 (s, 3H), 1.06 (d, $J = 6.9$ Hz, 3H), 2.19 (dd, $J = 12.0$, 5.8 Hz, 1H), 2.28 (dd, $J = 12.0$, 9.2 Hz, 1H), 2.80 (ddd, $J = 9.2$, 6.9, 5.8 Hz, 1H), 6.28 (ddd, $J = 8.2$, 7.4, 1.6 Hz, 1H), 6.80 (td, $J = 7.2$, 1.1 Hz, 1H), 6.83 (d, $J = 8.3$ Hz, 1H), 7.02 (d, $J = 8.2$ Hz, 1H), 7.24 (dd, $J = 7.2$, 1.5 Hz, 1H), 7.28 (d, $J = 8.4$ Hz, 1H), 7.35−7.43 (m, 3H), 7.53 (ddd, $J = 8.6$, 6.7, 1.4 Hz, 1H), 7.62−7.67 (m, 2H), 8.27 (dd, $J = 7.4$, 1.6 Hz, 1H), 8.80 (d, $J = 8.7$ Hz, 1H); ^{13}C NMR (100 MHz, $CDCl_3$) δ 0.5 (q), 3.4 (q), 21.5 (q), 35.3 (t), 40.9 (d), 64.1 (s), 66.4 (s), 122.9 (d), 124.4 (d), 125.4 (d), 125.5 (d), 126.0 (d), 126.6 (d), 126.9 (d), 127.2 (d), 128.1 (d), 128.3 (d), 129.2 (d), 131.2 (d), 131.3 (s), 132.3 (s), 132.4 (d), 134.3 (d), 134.7 (s), 135.9 (s), 138.1 (s), 138.9 (s), 143.1 (s), 144.7 (s); HRMS (ESI+) calcd for $C_{29}H_{27}S_2Si^+$ $[M + H]^+$ 467.1318, found 467.1312.

5,5-Dimethyl-10-(2-methyl-2,3-dihydro-1H-benzo[f]-thiochromen-1-ylidene)-5,10-dihydrodibenzo[b,e]siline ***4***. A mixture of episulfide **11** (0.10 g, 0.21 mmol) and copper bronze (0.14 g, 2.1 mmol) in *p*-xylene (3 mL) was heated at reflux for 14 h. The resulting mixture was passed through a short plug of silica using dichloromethane as eluent. Removal of the organic solvents followed by column chromatography (SiO_2), pentane/EtOAc = 100:1) afforded alkene **4** (81 mg, 87%) as a colorless solid. ^1H NMR (400 MHz, $CDCl_3$) δ 0.64 (s, 3H), 0.75 (s, 3H), 0.77 (d, $J = 7.0$ Hz, 3H), 2.92 (dd, $J = 11.7$, 4.0 Hz, 1H), 3.62 (dd, $J = 11.7$, 8.6 Hz, 1H), 4.15−4.20 (m, 1H), 6.28 (d, $J = 8.1$ Hz, 1H), 6.42 (t, $J = 7.6$ Hz, 1H), 6.75 (t, $J = 7.3$ Hz, 1H), 6.95 (dd, $J = 8.4$, 6.9 Hz, 1H), 7.12 (dd, $J = 8.1$, 6.9 Hz, 1H), 7.33 (t, $J = 7.3$ Hz, 1H), 7.37 (d, $J = 7.1$ Hz, 1H), 7.43 (t, $J = 7.6$ Hz, 1H), 7.44−7.49 (m, 2H), 7.58 (d, $J = 8.1$ Hz, 1H), 7.63 (d, $J = 8.5$ Hz, 1H), 7.67−7.71 (m, 2H); ^{13}C NMR (100 MHz, $CDCl_3$) δ −4.4 (q), −1.1 (q), 20.5 (q), 34.9 (d), 37.5 (t), 124.3 (d), 124.9 (d), 125.1 (d), 125.4 (d), 126.1 (d), 126.5 (d), 127.2 (d), 127.4 (d), 127.4 (d), 128.1 (d), 128.3 (d), 128.4 (d), 130.9 (s), 131.6 (s), 132.3 (d), 133.0 (d), 134.5 (s), 135.4 (s), 135.5 (s), 137.3 (s), 137.5 (s), 138.0 (s), 146.5 (s), 147.8 (s); HRMS (ESI+) calcd for $C_{29}H_{27}SSi^+$ $[M + H]^+$ 435.1597, found 435.1594.

HPLC Resolution. Resolution of the enantiomers of **1**−**4** was performed by HPLC (40 °C, flow rate 0.5 mL/min). Compound **1**: Chiralcel ODH column, 99.8:0.2 *n*-heptane/2-propanol, $t = 9$ min, 11 min. Compound **2**: Chiralpak ADH column, 99:1 *n*-heptane/2-propanol, $t = 11$ min, 13 min. Compound **3**: Chiralcel ODH column, 99.8:0.2 *n*-heptane/2-propanol, $t = 18$ min, 21 min. Compound **4**: Chiralcel ODH column, 99.9:0.1 *n*-heptane/2-propanol, $t = 18$ min, 23 min.

UV−vis and CD Spectroscopy. All spectra were recorded at rt using spectroscopic grade *n*-hexane as a solvent. Irradiation was performed using a UV lamp with $\lambda_{max} = 312$ nm. To ensure a photostationary state was reached, several spectra were recorded at set intervals until no further changes were observed.

Computational Chemistry. The Gaussian 09 program was used for geometry optimizations and the calculation of energies.[38] Initial geometries were optimized using semiempirical PM3. Geometry optimizations were performed on B3LYP/6-31G(d,p) using tight convergence criteria or M06-2X/6-31G(d,p) where indicated. To ensure minima and transition states were reached, frequency analyses of the obtained structures were evaluated; all minima had no imaginary frequencies, while all transition states were first-order. Energies reported are SCF energies unless noted otherwise. CD spectra were calculated using B3LYP/6-31++G(d,p). IRC calculations were performed using the Firefly QC package,[39] which is partially based on the GAMESS (US)[40] source code, using the Gonzalez−Schlegel second order method.

■ ASSOCIATED CONTENT

Ⓢ Supporting Information

Characterization data of new compounds, details on the spectroscopic studies and details on computational studies including Cartesian coordinates for all minima and transition states. This material is available free of charge via the Internet at http://pubs.acs.org.

■ AUTHOR INFORMATION

Corresponding Author

*E-mail: b.l.feringa@rug.nl.

Notes

The authors declare no competing financial interest.

■ ACKNOWLEDGMENTS

The authors thank The Netherlands Organization for Scientific Research (NWO-CW), the Royal Netherlands Academy of Sciences (KNAW), the European Research Council (ERC advanced grant 227897), and the Ministry of Education, Culture and Science (Gravity program 024.001.035) for financial support.

■ REFERENCES

(1) Leigh, D. A.; Zerbetto, F.; Kay, E. R. *Angew. Chem., Int. Ed.* **2007**, *46*, 72−191.

(2) Browne, W. R.; Feringa, B. L. *Nat. Nanotechnol.* **2006**, *1*, 25−35.

(3) Balzani, V.; Credi, A.; Venturi, M. *Chem. Soc. Rev.* **2009**, *38*, 1542−1550.

(4) Coskun, A.; Banaszak, M.; Astumian, R. D.; Stoddart, J. F.; Grzybowski, B. A. *Chem. Soc. Rev.* **2012**, *41*, 19−30.

(5) Koumura, N.; Zijlstra, R. W. J.; van Delden, R. A.; Harada, N.; Feringa, B. L. *Nature* **1999**, *401*, 152−155.

(6) Kelly, T. R.; De Silva, H.; Silva, R. A. *Nature* **1999**, *401*, 150−152.

(7) Fletcher, S. P.; Dumur, F.; Pollard, M. M.; Feringa, B. L. *Science* **2005**, *310*, 80−82.

(8) Tierney, H. L.; Murphy, C. J.; Jewell, A. D.; Baber, A. E.; Iski, E. V.; Khodaverdian, H. Y.; McGuire, A. F.; Klebanov, N.; Sykes, E. C. H. *Nat. Nanotechnol.* **2011**, *6*, 625−629.

(9) Perera, U. G. E.; Ample, F.; Kersell, H.; Zhang, Y.; Vives, G.; Echevarria, J.; Grisolia, M.; Rapenne, G.; Joachim, C.; Hla, S.-W. *Nat. Nanotechnol.* **2013**, *8*, 46−51.

(10) Kudernac, T.; Ruangsupapichat, N.; Parschau, M.; Maciá, B.; Katsonis, N.; Harutyunyan, S. R.; Ernst, K.-H.; Feringa, B. L. *Nature* **2011**, *479*, 208−211.

(11) Hernández, J. V.; Kay, E. R.; Leigh, D. A. *Science* **2004**, *306*, 1532−1537.

(12) Haberhauer, G. *Angew. Chem., Int. Ed.* **2011**, *50*, 6415−6418.

(13) Koumura, N.; Geertsema, E. M.; van Gelder, M. B.; Meetsma, A.; Feringa, B. L. *J. Am. Chem. Soc.* **2002**, *124*, 5037−5051.

(14) Koumura, N.; Geertsema, E. M.; Meetsma, A.; Feringa, B. L. *J. Am. Chem. Soc.* **2000**, *122*, 12005−12006.

(15) Biedermann, P. U.; Stezowski, J. J.; Agranat, I. *Eur. J. Org. Chem.* **2001**, 5−34 and references therein.

(16) Feringa, B. L.; Jager, W. F.; de Lange, B. *Tetrahedron Lett.* **1992**, *33*, 2887−2890.

(17) Biedermann, P. U.; Stezowski, J. J.; Agranat, I. *Chem.—Eur. J.* **2006**, *12*, 3345−3354.

(18) Assadi, N.; Pogodin, S.; Cohen, S.; Levy, A.; Agranat, I. *Struct. Chem.* **2009**, *20*, 541−556.

(19) Black, M.; Woodford, C.; Mills, N. S. *J. Org. Chem.* **2011**, *76*, 2286−2290.

(20) Piekarski, A. M.; Mills, N. S.; Yousef, A. *J. Am. Chem. Soc.* **2008**, *130*, 14883−14890.

(21) Pollard, M. M.; Klok, M.; Pijper, D.; Feringa, B. L. *Adv. Funct. Mater.* **2007**, *17*, 718−729.

(22) Conyard, J.; Addison, K.; Heisler, A.; Cnossen, A.; Browne, W. R.; Feringa, B. L.; Meech, S. R. *Nat. Chem.* **2012**, *4*, 547−551.

(23) Geertsema, E. M.; van der Molen, S. J.; Martens, M.; Feringa, B. L. *Proc. Natl. Acad. Sci. U.S.A.* **2009**, *106*, 16919−16924.

(24) van Delden, R. A.; ter Wiel, M. K. J.; Pollard, M. M.; Vicario, J.; Koumura, N.; Feringa, B. L. *Nature* **2005**, *437*, 1337−1340.

(25) ter Wiel, M. K. J.; van Delden, R. A.; Meetsma, A.; Feringa, B. L. *Org. Biomol. Chem.* **2005**, *3*, 4071−4076.

(26) Morin, J.-F.; Shirai, Y.; Tour, J. M. *Org. Lett.* **2006**, *8*, 1713−1716.

(27) Corey, J. Y.; Dye, M. J.; Farrell, R. L.; Mitchell, M. V. *J. Organomet. Chem.* **1978**, *153*, 127−135.

(28) Bickelhaupt, F.; Jongsma, C.; de Koe, P.; Lourens, R.; Mast, N. R.; van Mourik, G. L.; Vermeer, H.; Weustink, R. J. M. *Tetrahedron* **1976**, *32*, 1921−1930.

(29) Kazaryan, A.; Kistemaker, J. C. M.; Schäfer, L. V.; Browne, W. R.; Feringa, B. L.; Filatov, M. *J. Phys. Chem.* **2010**, *114*, 5058−5067.

(30) Zazza, C.; Mancini, G.; Brancato, G.; Barone, V. *J. Phys. Chem. Lett.* **2013**, *4*, 3885−3890.

(31) *Handbook of Photochemistry*; Montalti, M., Credi, A., Prodi, L., Gandolfi, M. T., Eds.; CRC Press: Boca Raton, 2006; pp 602−604.

(32) Klok, M.; Browne, W. R.; Feringa, B. L. *Phys. Chem. Chem. Phys.* **2009**, *11*, 9124−9131.

(33) Grimme, S.; Neese, F. *J. Chem. Phys.* **2007**, *127*, 154116.

(34) Klok, M.; Walko, M.; Geertsema, E. M.; Ruangsupapichat, N.; Kistemaker, J. C. M.; Meetsma, A.; Feringa, B. L. *Chem.—Eur. J.* **2008**, *14*, 11183−11193.

(35) Pérez-Hernández, G.; González, L. *Phys. Chem. Chem. Phys.* **2010**, *12*, 12279−12289.

(36) Grimme, S.; Ehrlich, S.; Goerigk, L. *J. Comput. Chem.* **2011**, *32*, 1456−1465.

(37) Agranat, I.; Tapuho, Y. *J. Am. Chem. Soc.* **1979**, *101*, 665−671.

(38) Frisch, M. J.; Trucks, G. W.; Schlegel, H. B.; Scuseria, G. E.; Robb, M. A.; Cheeseman, J. R.; Scalmani, G.; Barone, V.; Mennucci, B.; Petersson, G. A.; Nakatsuji, H.; Caricato, M.; Li, X.; Hratchian, H. P.; Izmaylov, A. F.; Bloino, J.; Zheng, G.; Sonnenberg, J. L.; Hada, M.; Ehara, M.; Toyota, K.; Fukuda, R.; Hasegawa, J.; Ishida, M.; Nakajima, T.; Honda, Y.; Kitao, O.; Nakai, H.; Vreven, T.; Montgomery, Jr., J. A.; Peralta, J. E.; Ogliaro, F.; Bearpark, M.; Heyd, J. J.; Brothers, E.; Kudin, K. N.; Staroverov, V. N.; Kobayashi, R.; Normand, J.; Raghavachari, K.; Rendell, A.; Burant, J. C.; Iyengar, S. S.; Tomasi, J.; Cossi, M.; Rega, N.; Millam, J. M.; Klene, M.; Knox, J. E.; Cross, J. B.; Bakken, V.; Adamo, C.; Jaramillo, J.; Gomperts, R.; Stratmann, R. E.; Yazyev, O.; Austin, A. J.; Cammi, R.; Pomelli, C.; Ochterski, J. W.; Martin, R. L.; Morokuma, K.; Zakrzewski, V. G.; Voth, G. A.; Salvador, P.; Dannenberg, J. J.; Dapprich, S.; Daniels, A. D.; Farkas, Ö.; Foresman, J. B.; Ortiz, J. V.; Cioslowski, J.; Fox, D. J. *Gaussian 09, Revision B.01*; Gaussian, Inc.: Wallingford, CT, 2009.

(39) Granovsky, A. A. *Firefly version 7.1.G*; http://classic.chem.msu.su/gran/firefly/index.html

(40) Schmidt, M. W.; Baldridge, K. K.; Boatz, J. A.; Elbert, S. T.; Gordon, M. S.; Jensen, J. H.; Koseki, S.; Matsunaga, N.; Nguyen, K. A.; Su, S.; Windus, T. L.; Dupuis, M.; Montgomery, J. A. *J. Comput. Chem.* **1993**, *14*, 1347−1363.